Fire Safety Journal 162 (2026) 104713

Contents lists available at ScienceDirect

Fire Safety Journal

journal homepage: www.elsevier.com/locate/firesaf

Coupling computer-vision house fuel load estimation with fire spread simulation in the Wildland–Urban interface

Yifei Ding [a,b,1], Nisha Saharan [c,1], Negar Elhami-Khorasani [c,*], Thomas Gernay [b], Yuxin Zhang [a], Xinyan Huang [a,e,**]

[a] Research Centre for Smart Urban Resilience and Firefighting, Department of Building Environment and Energy Engineering, The Hong Kong Polytechnic University, Hong Kong
[b] Department of Civil and Systems Engineering, Johns Hopkins University, Baltimore, MD, USA
[c] Department of Civil, Structural and Environmental Engineering, University at Buffalo, Buffalo, NY, USA
[e] State Key Laboratory of Climate Resilience for Coastal Cities, The Hong Kong Polytechnic University, Hong Kong

ARTICLE INFO

Keywords:
WUI fire
Residential fire load
SWUIFT
Lahaina fire
Fire spread simulation

ABSTRACT

Wildfires directly threaten human lives and properties in the wildland-urban interface (WUI). The quantity of combustible materials within houses is critical, yet variability in house fuel load remains unaccounted in current WUI fire modelling. This study integrates House Fuel Load (HFL) into the Streamlined Wildland–Urban Interface Fire Tracing (SWUIFT) simulation framework to examine its influence on WUI fire spread. HFL assessments were derived from computer-vision assessment of structural attributes and combined with standardized indoor fuel load values to calculate fully developed fire durations of ignited structures. We compared a baseline SWUIFT runs (fixed fire-duration configuration) with HFL-coupled cases under two pHRR scenarios of 100 kW/m^2 and 150 kW/m^2 in simulations of the 2023 Lahaina fire. Results indicate that although varied HFL modifies the theoretical heat release of individual structures, the WUI fire spread patterns and ignition statistics remain largely consistent. Sensitivity analysis further indicates that reducing burning time below 60 min substantially inhibits fire spread, whereas durations beyond 100 min have limited additional influence. Overall, the HFL-based method provides reasonable estimates of residential burning time, and the corresponding simulated fire spread paths align closely with the real event, supporting the applicability of the approach.

1. Introduction

Human life and property are increasingly threatened by wildland fires, especially in the wildland-urban interface (WUI) area, where residential structures coexist with surrounding vegetation. Till November 2025, a total of 706,369 wildfires occurred all over the word, including 69,444 in Asia, 42,821 in North America, 36,460 in Australia, and 18,976 in Europe [1]. The fraction of global fires that occur in WUI areas increased by about 23% from 2005 to 2020 [2]. When a wildfire reaches WUI communities, residential structures are susceptible to ignition and destruction [3]; for example, 4552 structures were destroyed in 2024 in the United. More recently, the 2025 Southern California wildfires caused 31 direct fatalities [4], and destroyed over 14,000 structures with damage extending beyond the WUI into urban neighborhoods [5]. These events underscore not only the increasing frequency and intensity of wildfires, but also critical vulnerabilities in the built environment, particularly in WUI communities [6].

To reduce structural vulnerability in WUI fires, building codes and material standards have incorporated ignition-resistant requirements [7–9]. However, these standards are often evaluated under simplified testing conditions that do not reflect the coupled, multi-factor fire risk in real WUI scenarios [10,11]. Designing adaptive and effective mitigation strategies and structural protections requires a systematic understanding and modelling of the entire fire spread process from wildland to

This article is part of a special issue entitled: FISJ_IAFSS 2026 published in Fire Safety Journal.

* Corresponding author.
** Corresponding author. Research Centre for Smart Urban Resilience and Firefighting, Department of Building Environment and Energy Engineering, The Hong Kong Polytechnic University, Hong Kong.
E-mail addresses: negarkho@buffalo.edu (N. Elhami-Khorasani), xy.huang@polyu.edu.hk (X. Huang).

[1] These authors contributed to the work equally and should be regarded as co-first authors.

https://doi.org/10.1016/j.firesaf.2026.104713
Received 23 September 2025; Received in revised form 8 January 2026; Accepted 8 March 2026
Available online 13 March 2026

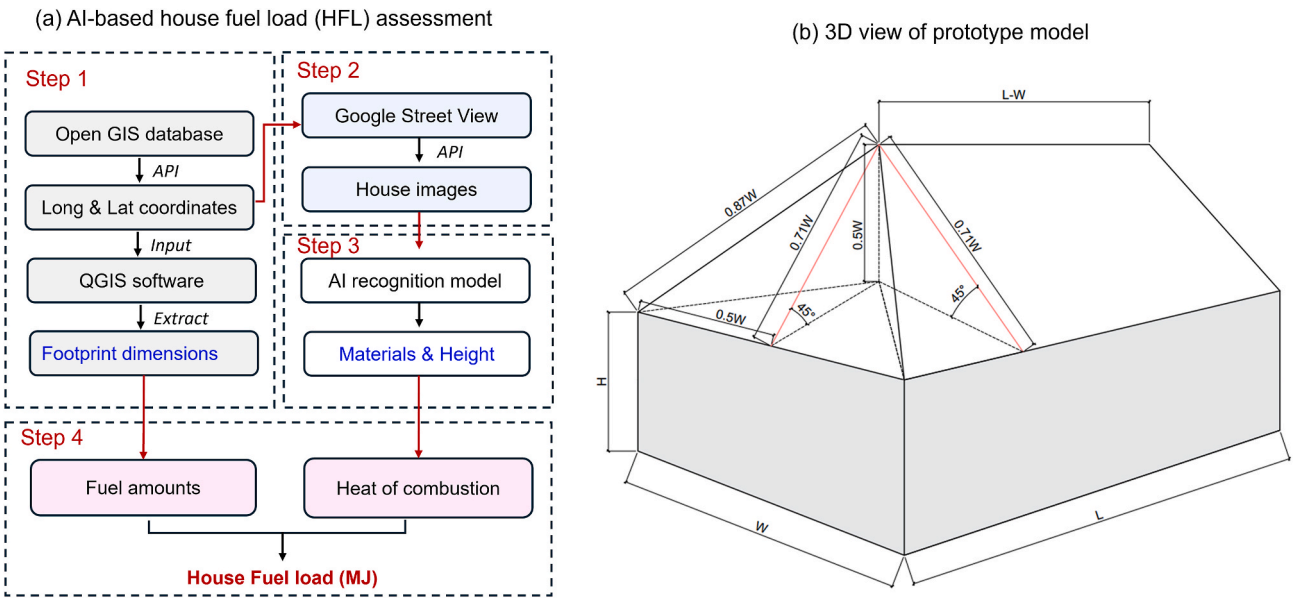

Fig. 1. (a) Workflow for batch assessment of house fuel load (HFL), (b) 3D view of a typical prototype house model in wildland-urban interface (WUI).

community. The major fire propagation modes among vegetation and structures in WUI fire are thermal radiation [12], direct flame contact [13], and firebrand (or ember) exposure [14]. Laboratory-scale experimental studies are gradually characterizing and quantifying these three spread mechanisms [15–20], which provide critical input parameters for fire modeling and simulations. Post-fire investigations further show that the ignition probability and damage level of structures in the WUI fire are affected by their construction features (e.g., construction type, materials of roof, wall, deck, fence, etc.) [21]. A particularly important but unexplored factor is the house fuel load (HFL), defined as the amount of combustible materials, including structural fuel load (SFL) from fixed building components and indoor fuel load (IFL) from movable contents (e.g., furniture and appliances). While the effects of IFL on compartment fire behaviors [22] and fire protection systems [23] have been studied, the current WUI fire risk assessment rarely accounts for the global HFL.

Modelling the fire spread from vegetation to structures and between structures in WUI remains in an exploratory phase [24–26]. The relative contributions of different fire spread mechanisms and ignition modes vary widely among different fire events. Several approaches have been proposed to simulate fire spread at the community scale. For example, the Streamlined Wildland–Urban Interface Fire Tracing (SWUIFT) model, developed by one of the authors' research groups, incorporates both radiation and firebrand-driven ignition. In this model, firebrand generation from structures is estimated using experimental statistics and roof area [27] with each combustion cell assumed to have a constant firebrand generation time. Qin et al. [25] introduced an alternative framework in which the heat release rate (HRR) serves as the governing parameter for firebrand generation; however, the model applies a constant HRR to all structural cells. Purnomo' model [28] assumes that fully developed fire duration of an ignited structure cell is 1 min, with a peak heat release rate per structural area of 150 kW/m^2, where the HRR contributes to fire spread for full duration not just the peak. The model considers direct flame contact and thermal radiation but relies on proportional area-based transfer coefficients. Despite these efforts, current models neglect HFL as an input variable, thereby overlooking structure-specific differences in fire behavior associated with varying fuel quantities. Capturing such variability requires incorporating HFL into spread models, while still maintaining computational efficiency.

At present, there are few well-established statistical datasets or developed empirical framework to define house HFL, particularly SFL, and their influence on fire development in WUI communities. In contrast, IFL has been more extensively studied, with non-linear models developed to describe its correlation with compartment fire dynamics [29,30]. For instance, Eurocode specifies a reference IFL density of 780 MJ/m^2 for residential buildings [31]. However, quantifying SFL poses greater challenges despite its potential role as a critical source of fuel in WUI fire scenarios. In our preliminary work [32], we developed an SFL assessment method based on house image recognition and remote sensing data, which enables the identification of structural surface materials and the calculation of total heat potential through physical equations. As an extension of our previous work, the present study aims to incorporate and verify the influence of variable HFL on fire spread modeling by coupling HFL data into WUI fire spread simulations.

Here, we propose an HFL-coupled SWUIFT model to simulate WUI fire spread. The method first estimates SFL through AI-based recognition of house images combined with remote sensing data and calculates IFL based on the Eurocode value. The resulting HFL values are then used to determine the fully developed duration of ignited structures. A spatial distribution matrix of fire durations is superimposed onto community-scale input maps of structures and vegetation to perform SWUIFT simulations. Key evaluation metrics include the fire spread pattern over time and structure ignition statistics to quantify the effects of HFL. To assess the reliability of the proposed method, the process is applied to the 2023 Lahaina Fire as a case study, simulating a historical WUI fire in the United States and evaluating model performance against field observations and results from the original SWUIFT framework.

2. Methodology

2.1. House fuel load assessment

In this section, the workflow of batch assessment of HFLs in a target WUI community is introduced, including four main steps: (1) footprint dimension assessment from GIS data, (2) street house image collections, (3) structural attribute recognition by an AI model, and (4) HFL calculations, as illustrated in Fig. 1(a).

In Step 1, the target community is searched through the public GIS database, i.e., OpenStreetMap [33] and Bing map [34], from which all residential structures are retrieved. The geographic coordinates (longitude and latitude) of each building centroid are recorded. These data are then processed in QGIS to extract footprint parameters denoted as $[P, A, W, L]$ representing perimeter, area, width, and length of the

Table 1
Fuel load per unit area of different materials of roof and wall.

Component	Material	Fuel load density (MJ/m^2)
Siding wall	Wood	219.1
	Metal	93.6
	Vinyl	93.6
	Brick	93.6
Roof Shingle	Wood	340.1
	Asphalt	288.3
	Concrete	288.3
	Tile	288.3
	Metal	288.3

footprint bounding box, respectively. In Step 2, the recorded coordinates are input into Google Street View, where house street images are batch-downloaded using a free Application Programming Interface (API) key. In Step 3, the collected images are analyzed using a pre-trained convolutional neural network (CNN) based on the ResNet-50 architecture to automatically identify key structural attributes.

The output of this AI recognition process is a three-dimensional vector denoted $[M_r, M_w, n]$, where M_r is the material of the roof surface, M_w is surface material of the wall, and n is the number of stories. Based on the compiled dataset, SFL and IFL are subsequently calculated following the unified prototype model illustrated in Fig. 1(b). The surface area of the roof material is calculated as Eq. (1),

$$A_{roof} = (L - W + L) \times 0.71W \times \frac{1}{2} \times 2 + W \times 0.71W \times \frac{1}{2} \times 2 \quad (1)$$

After combining the terms,

$$A_{roof} = 1.414 \times L \times W \quad (2)$$

The surface area of wall material is calculated as

$$A_{wall} = P \times H \quad (3)$$

where P is the perimeter of the building footprint, and H is the building height.

After identifying the material types (e.g., wood, vinyl, etc.) of the roof and wall, the corresponding fuel load is calculated in Step 4 by multiplying the material-specific fuel load density as:

$$SFL = A_{roof} \times q_{roof} + A_{wall} \times q_{wall} \quad (4)$$

where, q_{roof} and q_{wall} are the fuel load per unit area of roof and wall (shown as Table 1), respectively.

In terms of IFL, we adopt the characteristic reference value for residential design provided by Eurocode, specified as 780 MJ/m^2. The IFL is calculated as a function of the footprint area (A) and the number of stories (n), denoted as,

$$IFL = 780 \times A \times n \quad (5)$$

Lastly, HFL equals the sum of SFL and IFL.

2.2. WUI fire spread modelling (SWUIFT)

SWUIFT [26] is a semi-empirical model that simulates fire spread in WUI environments by considering thermal radiation and firebrand spotting mechanisms. The validity and reliability of SWUIFT have been demonstrated in several major events, including the 2018 Camp Fire [35], the 2021 Marshall Fire [36], and the 2023 Lahaina Fire [37]. The model represents the spatial layout of a community using a rasterized grid of vegetation, structures, and non-combustible cells, each with dimensions of 10 m × 10 m. SWUIFT accounts for the uncertainties in fire spotting, ignition criteria, and the probability of structural ignition. Likelihood of ignition is assessed using either publicly available data (e.g., occupancy type, square footage) or through detailed community inspections (e.g., parcel-level data on roofing type, siding material,

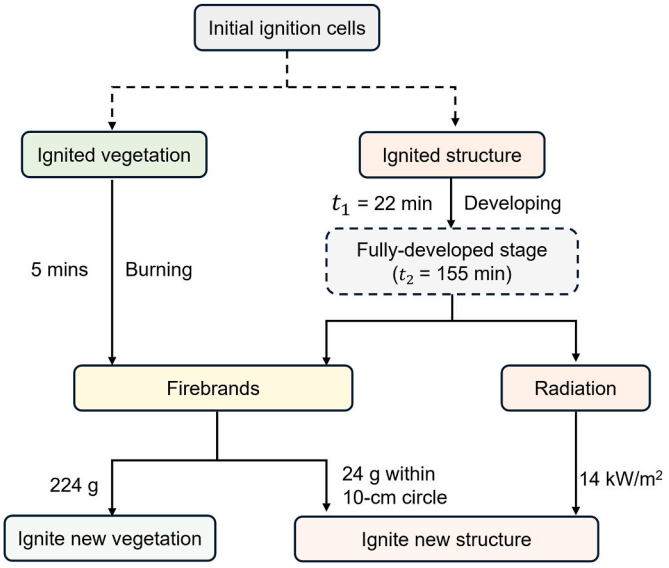

Fig. 2. Flowchart of original SWUIFT with default deterministic ignition criteria.

number of windowpanes, decks, fences, defensible spaces). In its original version, SWUIFT does not account for differences in building fuel load, treating all cells as 10 m × 10 m × 3 m burning units.

The SWUIFT model integrates input on wildland fire spread (e.g., from WRF-Fire or FARSITE) and updates fire propagation within a community at 5-min intervals. As illustrated in Fig. 2, simulation inside the community begins with ignition cells, typically resulting from fire spotting originating in the wildland. The ignitions inside the community may occur in vegetation or structures.

The ignited vegetation does not contribute thermal radiation but serves as a source of firebrands. Each vegetation cell burns for 5 min (one time step), and ignition occurs when the accumulated firebrand mass exceeds 224 g.

Ignited structures follow the compartment fire development process, including developing stage (t_1), fully-developed or stable-burning stage (t_2), and decay stage (t_3). The durations of these stages are 22 min, 155 min, and 140 min, respectively. A structural cell contributes to firebrand generation and thermal radiation only during the fully developed stage.

Firebrands produced by both structures and vegetation can ignite new cells (structures or vegetation). For structural ignition in SWUIFT setup, deposition of more than 24 g of firebrands within a 10-cm diameter is required [38]. Firebrand transport is governed by wind direction and probability distributions: a lognormal distribution is applied in the downwind direction, while a normal distribution is applied laterally. The total number of firebrands generated from a structure in a given time step (5 min) is derived from experimental statistical data, as expressed in Eq. (6):

$$n_b = \frac{306.77 e^{0.1879v} A_{roof}}{n_{t2}} \quad (6)$$

where v is the wind speed in m/s, and A_{roof} is roof area m^2, and n_{t2} represents the number of time steps in a fully-development stage of fire, which is set to 31.

According to the previous research [39,40], the critical ignition fluxes across and along the wood grains are 12.0 kW/m^2 and 9.0 kW/m^2, respectively. Therefore, the critical heat flux for structural ignition in SWUIFT is set at 14 kW/m^2 considering tiling or finishing, which is slightly larger than the reported values for bare materials in tests. Structures located within ±90° of the emitting surface, with respect to the wind direction, receive thermal radiation. The thermal radiative flux received at a given cell is determined at every time step by Eq. (7):

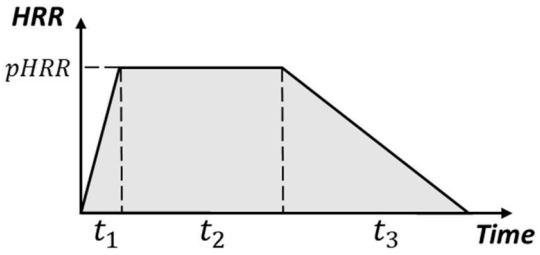

Fig. 3. Idealized HRR-time curve of an ignited residential structure.

$$\dot{q}'' = \phi \varepsilon_e \sigma T_e^4 \tag{7}$$

where $\dot{q}''$ is the radiative heat flux in W/m^2, ϕ is the configuration factor (view factor), ε_e is the emissivity of the emitting surface, σ is the Stefan-Boltzmann constant, and T_e is the absolute temperature of the emitting surface in K.

2.3. Modeling wildfire spread with house fuel load

This study aims to validate the influence of HFL on WUI fire spread modeling. To achieve this, the HFL data of individual structures obtained in Section 2.1 are integrated into the SWUIFT framework by modifying the combustion duration, which is directly governed by the respective HFL. The total heat release over time, i.e., the area under the curve shown in Fig. 3, is assumed to equal the HFL under complete combustion conditions as calculated in Eq. (8),

$$HFL = \int HRR\, dt = \left(\frac{1}{2}t_1 + t_2 + \frac{1}{2}t_3\right) pHRR \tag{8}$$

where, t_1, t_2, t_3 represent the durations of growth stage, fully developed stage, and decay stage in minutes, and *pHRR* represents peak heat release rate.

If we assume *pHRR*, t_1, and t_3 are constant, the duration of the fully developed stage for each structure cell to generate firebrand and thermal radiation can be calculated as:

$$t_2 = \frac{HFL}{pHRR} - \frac{t_1 + t_3}{2} \tag{9}$$

In this work, t_1 is assumed to be 22 min and t_3 is assumed to be 140 min. Two values of peak heat release rate per unit area (HRRPUA) are assigned for structural cells, namely 100 kW/m^2 and 150 kW/m^2, and a sensitivity analysis is performed to evaluate the influence of HRRPUA. pHRR is then calculated by Eq. (10),

$$pHRR = HRRPUA \cdot A \cdot n \tag{10}$$

where, A is the footprint area, and n is the number of house stories.

Eq. (6) is updated and the total number of generated firebrands from a structure in one simulation time step (5 min) is calculated based on t_2, shown as Eq. (11). Similarly, the duration over which a structure contributes to fire spread via thermal radiation is adjusted based on t_2.

$$n_b = \frac{306.77 e^{0.1879v} A_{roof}}{t_2/5} \tag{11}$$

Based on the assessed HFLs of all residences obtained from GIS data and the AI model, the fire duration of each individual structural cell can be calculated. The resulting distribution matrix of fire duration is then superimposed onto the community map raster to conduct SWUIFT simulations.

2.4. Case study: the 2023 Lahaina Fire

In this work, we conduct HFL-coupled SWUIFT simulation for the 2023 Lahaina fire in Maui, Hawaii, as the case study. The spatial domain for the analysis covers the coordinates 20.854 (South), 20.903 (North), −156.690 (West), −156.660 (East), with a total area of 1729 ha, shown as Fig. 4(a). The domain covers the area affected by the Lahaina Fire, part of a series of devastating wildfires on the Hawaiian island of Maui, ignited on August 8, 2023, fueled by strong winds from Hurricane Dora and drought conditions. The fire rapidly spread through Lahaina, leading to 102 fatalities and destroying over 2000 structures. The Lahaina Fire was the deadliest wildfire in the United States since 1918 [41].

Vegetation landcover data were obtained from the LANDFIRE fuel maps, while building locations were extracted from Microsoft's United

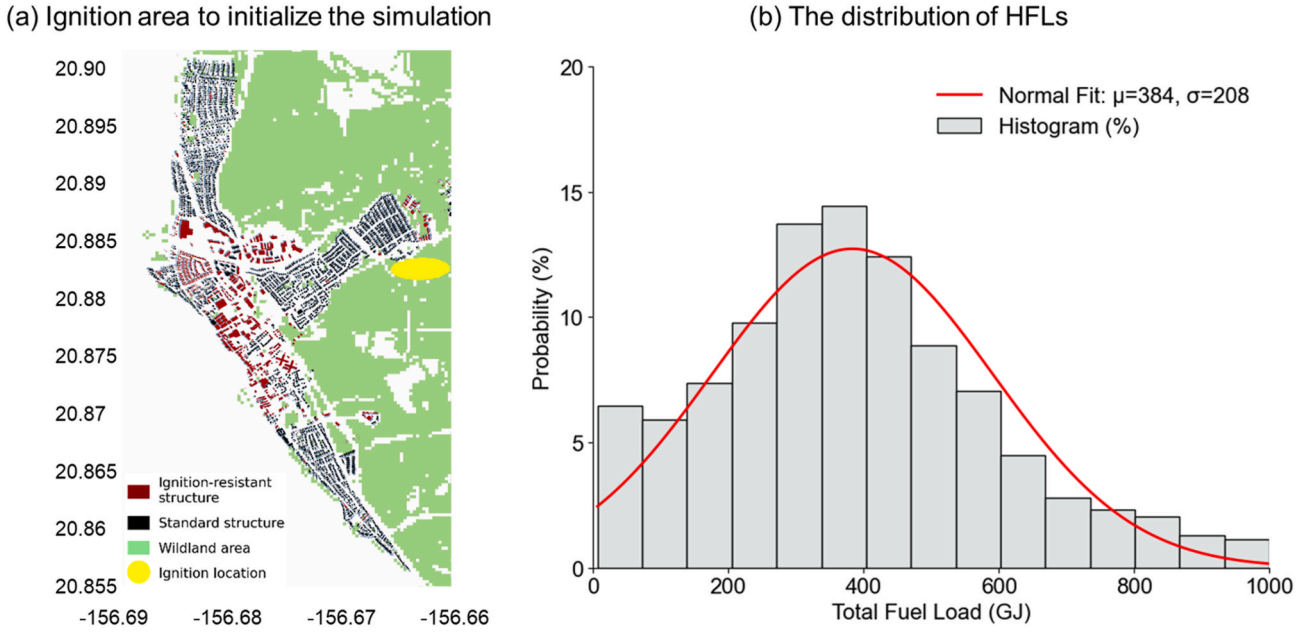

Fig. 4. (a) Ignition area to initialize the simulation, along with the building locations and classifications. (b) The probability distribution of estimated HFLs in the study domain.

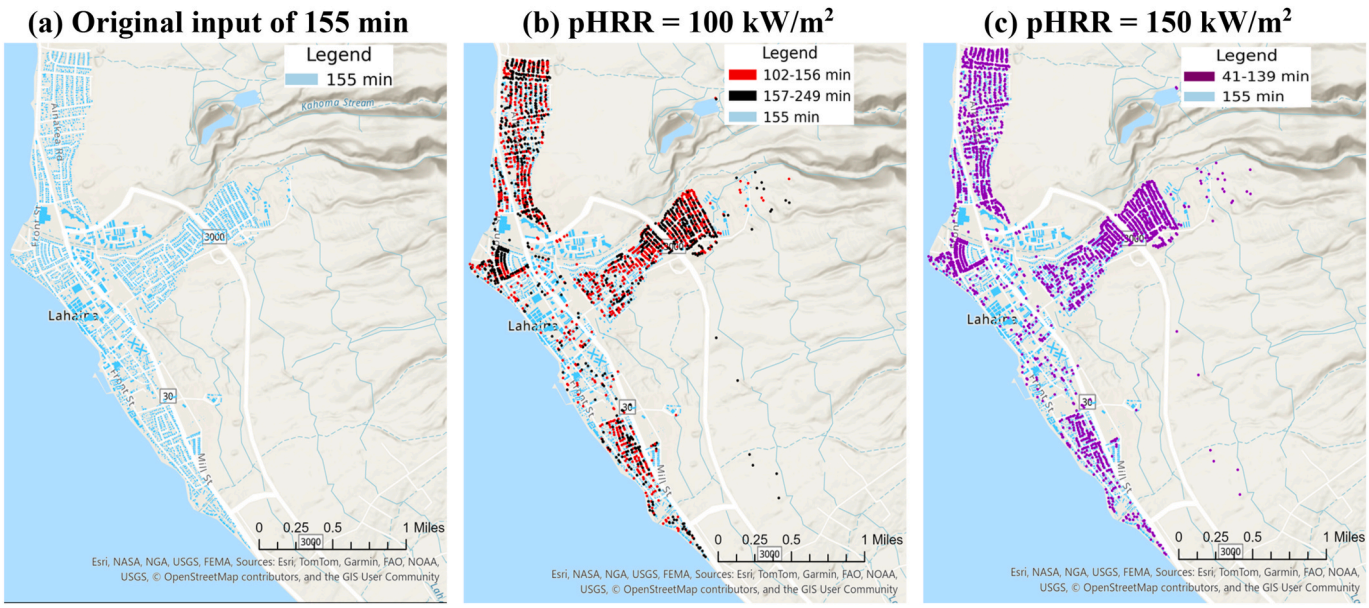

Fig. 5. Comparison of the duration of the fully developed phase, during which a structure contributes to thermal radiation and fire spotting: (a) original input of 155 min, (b) HFL-based calculation with pHRR = 100 kW/m^2, and (3) HFL-based calculation with pHRR = 150 kW/m^2.

States Building Footprints database and OpenStreetMap. The simulations were driven by high-resolution wind fields generated with the WRF model [42]. The fire ignition was approximately located south of Lahainaluna Road, near the community, at 3:15 p.m. HST [43]. Because the ignition occurred in close proximity to the community, SWUIFT was applied as the sole simulator, without the need for an external wildland fire spread model [44].

SWUIFT differentiates between ignition-resistant structures, which have a lower probability of ignition based on construction features, and standard structures, which ignite once thresholds for thermal radiation or fire spotting are reached. For ignition-resistant structures, the probability of ignition is set at 0.3 for both thermal radiation and fire spotting [44], compared to standard structures.

Ignition-resistant structures are identified using detailed parcel-level inspection data where available, or by applying proxies (e.g., occupancy type) from publicly available datasets when such information is not accessible, shown as Fig. 4(a). In Lahaina, most residential structures are classified as standard. The exception is residential buildings constructed in or after 2020. These newer structures were reviewed through satellite and street-level imagery and manually classified as ignition-resistant if they incorporated fire-resistant features such as non-combustible roofing, siding, or decking. The 2020 cutoff year was selected based on a conservative assessment of the local building code environment, which indicates that only the most recent constructions integrate non-traditional fire-resistant characteristics. Although Hawaii has adopted the 2018 International Building Code and the 2018 International Residential Code, enforcement is carried out at the county level [45].

Within the study area, two clusters of recent construction were identified. The first is the Kahoma village community, located centrally in Lahaina near the Kahoma stream channel. Structures in Kahoma village were classified as ignition-resistant, as they featured Class A roof coverings, non-combustible wall claddings, high wind-rated off-ridge attic vents, and lower densities of inter-building connective fuels. The second is a cluster of houses on the west end of Komo Mai Street, which were classified as standard, as they retained traditional combustible exterior materials.

In summary, all residential buildings in Lahaina are classified as standard, except those in Kahoma village, which were identified as ignition resistant. Most non-residential structures (e.g., commercial) were assumed to be ignition-resistant. Further details are provided in Ref. [44].

3. Results and discussion

3.1. HFL estimation for predicting fire spread in the Lahaina Fire

The procedure described in Section 2.1 was applied to estimate the HFL for structures within the study domain in Lahaina. Estimates were generated for 1910 residential structures, while commercial structures with large footprints (over 500 m^2) were excluded. The estimated results of HFL are shown as Fig. 4(b), where the histogram of the data and a fitted normal curve show that the estimated values of HFL follow an approximately normal distribution. The mean value of HFL is 384 GJ with a standard deviation of 208 GJ, and most structures fall within the range of 200–500 GJ. Although extreme values are less frequent, the presence of high-HFL structures (larger than 600 GJ) and low-HFL structures (lower than 200 GJ) may affect overall fire spread in this community. The statistical results show the reasonable variability of the HFL values in Lahaina, which can be coupled into WUI fire spread simulations to verify their influences.

Using Eq. (9), the duration (t_2) for which each structure contributes to fire spread through thermal radiation and fire spotting was then evaluated. The AI algorithm of Section 2.1 was specifically developed for application to residential structures. Accordingly, the process was applied only to residential buildings with floor areas between 140 m^2 and 500 m^2. Floor area was used as a proxy to identify timber-frame construction, consistent with prior SWUIFT studies [44]. In Eq. (9), the variable t_2 is a function of the pHRR. For this study, t_2 was calculated using two pHRR values: 100 kW/m^2 and 150 kW/m^2. As expected, the duration of the fully developed phase decreases with increasing pHRR.

Fig. 5 compares the calculated durations of the fully developed stage for these two pHRR values with the default SWUIFT value of 155 min. The probability distribution of durations of the fully developed stage is shown as Fig. S1 in Appendix. When pHRR is set to 100 kW/m^2, 56% of t_2 values are ranging from 102 min to 156 min and 44% of are ranging from 157 min to 249. When pHRR increases to 150 kW/m^2, all structures' t_2 are within 139 min, which are notably shortened compared to the default value of SWUIFT (155 min) under the assumed pHRR. It indicates that different HFL assumptions affect the duration of a single-building fire, but the differences remain within a reasonable range. The

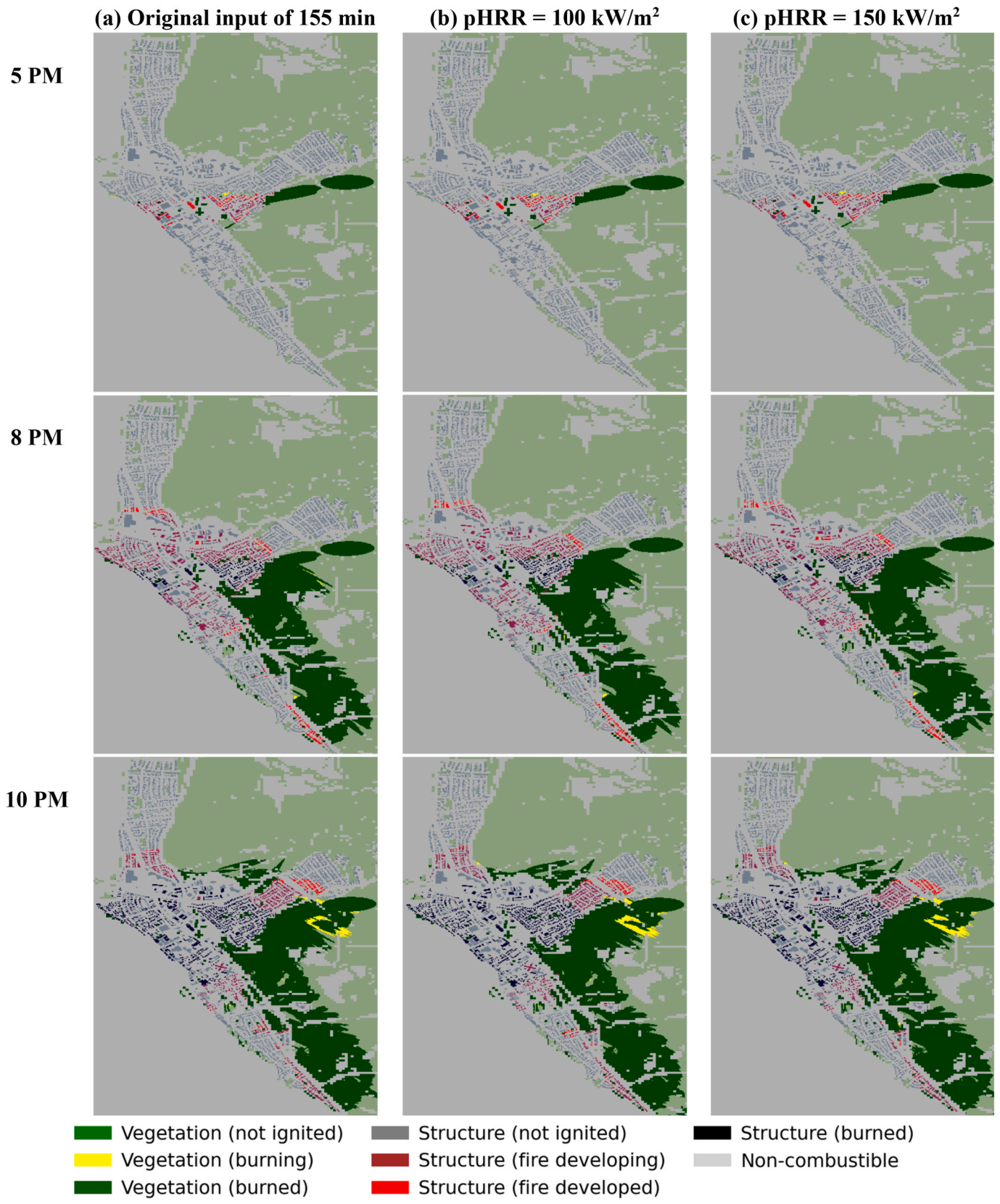

Fig. 6. Comparison of simulation results for the three considered cases, (a) original input of 155 min, (b) HFL-based calculation with pHRR = 100 kW/m^2, and (3) HFL-based calculation with pHRR = 150 kW/m^2.

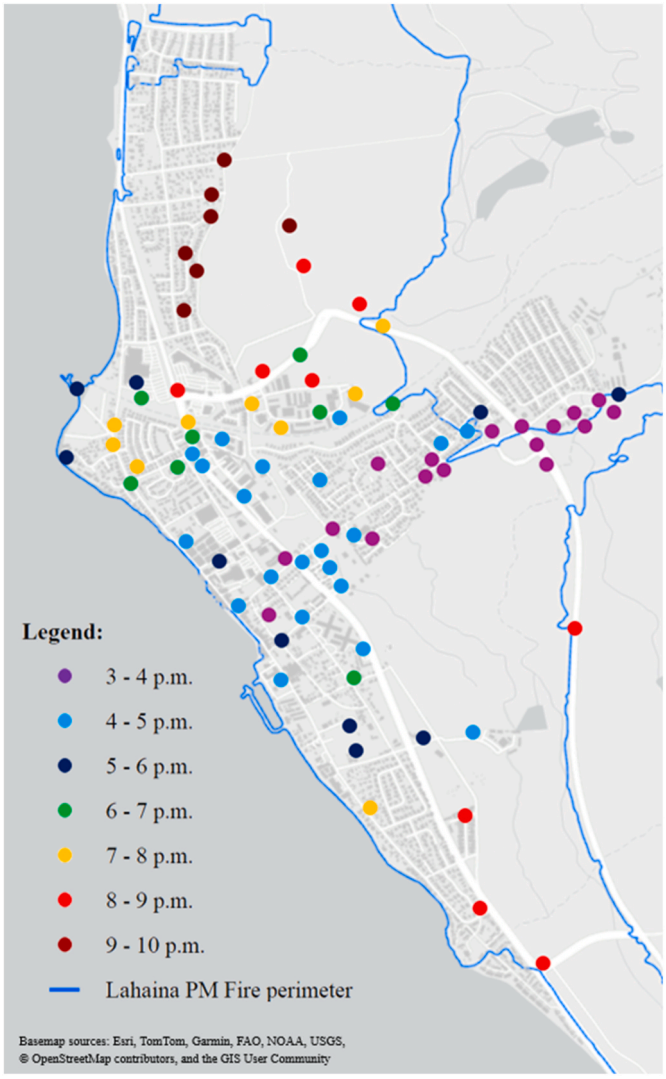

Fig. 7. Active fire observations generated from the Lahaina Fire Comprehensive Timeline Report (Phase 1) published by the Fire Safety Research Institute (credit: Szasdi Bardales, F., 2025 [44]).

magnitude of the calculated t_2 values is as expected, given the much larger average HFL (384 GJ) of the surveyed residential buildings compared with a group of 1/3-scale reduced-size house fire tests conducted by Himoto et al. [46]. In his tests, 15 wooden model houses with footprint area of 12.96 m^2 were burned. The average HFL of these house models is only 7.3 GJ, and average duration of fully-developed stage is 3.2 min. The comparison results show that the increase of fire duration aligns with scale effect where larger fuel loads naturally lead to longer fully-developed burning durations.

3.2. Fire spread simulation for the lahaina case study

Fig. 6 presents the fire spread simulation results for the three cases defined in Fig. 5, shown at three different time stamps (5 p.m., 8 p.m., and 10 p.m.). Overall, the differences among the three cases are minimal. All cases produce a similar fire spread path, consistent with documented observations from the real event, as reported by the Fire Safety Research Institute (FSRI) [47] and illustrated in Fig. 7. Finally, Fig. 8(a) summarizes the corresponding number of ignited structures at each critical time.

In each case, the fire reaches the historic town of Lahaina by approximately 5:00 p.m., though the simulations slightly underestimate the extent of fire progression compared with field observations. By 8:00 p.m., however, the simulated fire spread catches up, extending both north and south of the historic town. At this time, the extent of fire spread is similar across all three cases, with 1,402, 1,411, and 1392 ignited structures for two baselines of pHRRPUA = 100 kW/m^2 and 150 kW/m^2 cases, respectively.

Field data on the number of burning structures over time are not available; however, the results indicate that the HFL-based method provides reasonable estimates of residential fuel load densities. The simulated fire spread paths align closely with the real event, supporting the applicability of the approach.

3.3. Sensitivity of simulations to duration of thermal contribution to fire spread

The cases presented in Section 3.2 show minimal differences in the results when different pHRR values are considered. In this section, multiple simulations were conducted in which the duration of the fully developed phase, t_2, was fixed for all structures in the domain. The variable t_2 varied between 20 and 140 min, as summarized in Fig. 8(b).

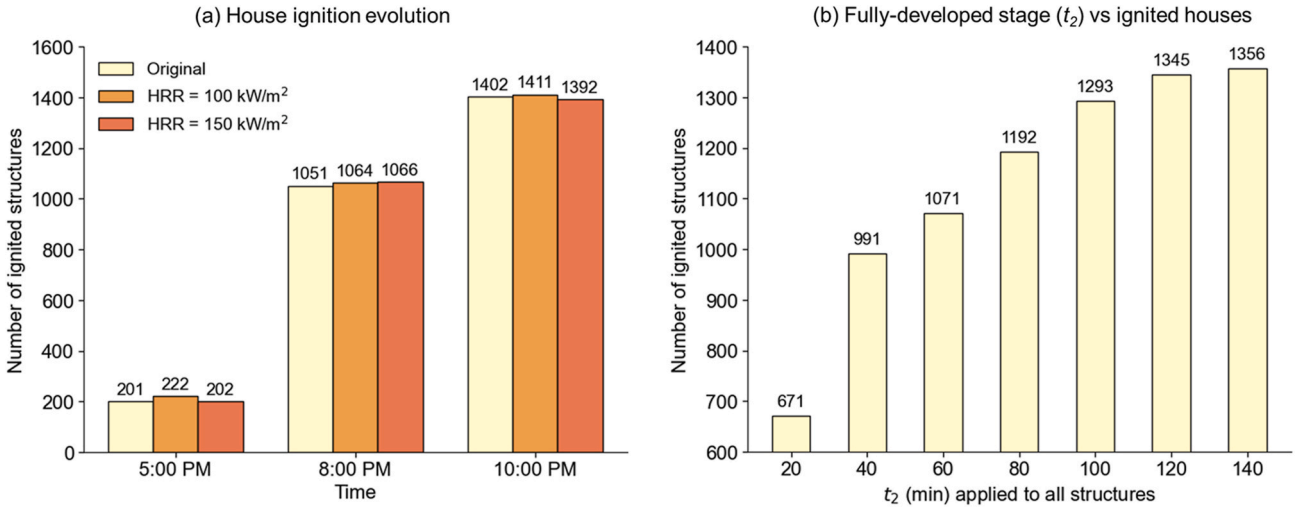

Fig. 8. (a) Growing ignited structures over time for different simulated fire scenarios, (b) Number of ignited structures as a function of fixed duration (t_2) applied to all structures.

By comparison, the calculated t_2 values ranged from approximately 100-250 min for a pHRR of 100 kW/m^2 and about 40-140 min for a pHRR of 150 kW/m^2.

Fig. 8(b) indicates that shorter durations (lower than 100 min) for all structures in the domain led to fewer ignited structures. For durations above 120 min, however, the change in the number of ignited structures tended towards saturation with only a minor increase. This analysis confirms that the fire spread model is sensitive to the lower limit of the available fuel and the corresponding duration during which a structure contributes to thermal radiation and fire spotting. When combustion time is much longer, the overall fire spread is dominated by other factors.

3.4. Discussion of modeling results

The simulation results indicate that variations in the estimated fire fully developed duration of burning structure (t_2) derived from different HFL assumptions have a limited impact on the overall fire spread results. While higher HFLs with longer burning durations increase the theoretical energy release of individual structures, the regional-scale WUI fire spread simulation in the Lahaina case study shows that this effect is not significant.

The reasons for this result include several aspects. Firstly, in the Lahaina case, strong winds and the continuous distribution of fuels provided sufficient conditions for rapid fire spread, driving flames and flying firebrands, where variations in individual HFL and corresponding burning time become less significant under our pHRR setups (100 kW/m^2 and 150 kW/m^2) once burning time increases to a threshold. Even if the burning time of some structures is very long, the overall fire line still advances rapidly along the primary wind direction. Once a structure has made a sufficient contribution to fire spread in its surroundings through thermal radiation in its immediate vicinity and fire spotting at greater distances, it may continue burning but would not further influence the overall fire spread pattern. Secondly, sensitivity analysis of t_2 indicates the presence of a threshold effect. When t_2 decreases to a certain value (e.g., lower than 60 min), the ignited structure cannot sustain long-term and stable thermal radiation and firebrand generation to its surrounding fuels, leading to an obvious suppression effect on fire spread. However, once the stable-burning stage (t_2) exceeds a certain threshold of approximately 100 min, additional burning time cannot significantly provide extra contribution of fuel ignitions, as the surrounding structures have already been ignited when the fire line reaches. In other words, once a burn time reaches the fundamental level required to maintain the fire propagation criteria, extending t_2 merely increases redundant heat release with very limited impact on regional fire spread. Thirdly, simulations indicate that the dominant factor in fire spread is not the total energy released by individual structures, but rather the spatial relationships among structures and the ignition timing during the advancing fire line, which is also proved by other parametric study [48]. When the fire line rapidly passes through, what is most critical is whether structures can be ignited, rather than how long the structure can continuously burn. However, the observed sensitivity of certain parameters e.g., the threshold effect of t_2 is specific to the setups of SWUIFT, and other models employing different assumptions may exhibit different sensitivities.

Accurately inputting wind conditions, topography, and spatial configurations of structures and vegetation will be more significant for enhancing simulation reliability than refining individual HFL. Moreover, when real measured HFL data is lacking, AI-based HFL values can satisfy the prediction purposes for WUI fire modelling, and excessive precision in HFL assessments is not necessary for current fire spread simulations. Additionally, variations in structural burning time cannot dominate large-scale fire spread for high HFL community, but HFL and corresponding overall fire duration are also very important parameters for regional smoke and temperature distribution, toxic gas emissions, and short and long-term impacts on environment. Future research about WUI fire spread predictions is recommended to pay more attention to the modeling of fire spread channels, for example, the generation, propagation, and ignition effects of firebrands on different construction materials, which are primary factors driving rapid structure-to-structure spread in WUI fire.

4. Conclusions

This study assessed the role of house fuel load (HFL) in WUI fire spread simulations through the application of an HFL-coupled SWUIFT simulation to the 2023 Lahaina Fire. HFLs provides a realistic input for estimating residential burning time and supported simulated fire spread paths and perimeter align closely with the real observation. Given the comparative analyses at one case study, it found that variations in high HFL and the corresponding calculated fully-developed fire duration have a limited impact on the overall fire spread results. The major reason is that fire spread rate slows down if the HFL values resulted in small fire duration (lower than 60 min), while the extended fire duration (over 100 min) only makes structure release more redundant heat when it exceeds a threshold, which has a relatively negligible effect on the already ignited surrounding structures.

Based on the analysis, the major findings and recommendations include the following,

1. AI-estimated HFL values are sufficient to capture realistic ranges of burning durations and satisfy the fundamental requirements of WUI fire modelling. Excessive precision in HFL assessments is not efficient for computational resources.
2. Environmental conditions and fuel distribution are dominant factors for WUI fire spread. Therefore, accurately capturing wind conditions and spatial configurations of fuels will be more significant than refining individual HFL.
3. Future research is suggested to pay more attention to fire spread mechanisms and ignition effects on different construction materials and fire-resistant protection structures, instead of the variability of individual structures.

In conclusion, the integration of HFL into WUI fire modeling enhances the physical realism of structural combustion representation but does not substantially alter community-scale fire spread under wind-driven conditions. This outcome affirms that large-scale propagation is governed by macro-environmental factors rather than distinct structural burning durations. Accordingly, WUI fire risk mitigation strategies should prioritize environmental and spatial management while using HFL estimation as a complementary but not decisive parameter of modelling input under constrained computational-source conditions.

CRediT authorship contribution statement

Yifei Ding: Writing – original draft, Visualization, Software, Methodology, Investigation, Formal analysis. **Nisha Saharan:** Writing – original draft, Visualization, Software, Methodology, Investigation, Formal analysis. **Negar Elhami-Khorasani:** Writing – review & editing, Supervision, Methodology, Funding acquisition, Formal analysis, Conceptualization. **Thomas Gernay:** Writing – review & editing, Supervision, Methodology, Formal analysis, Conceptualization. **Yuxin Zhang:** Writing – review & editing, Supervision. **Xinyan Huang:** Writing – review & editing, Supervision, Methodology, Funding acquisition, Formal analysis, Conceptualization.

Declaration of competing interest

The authors declare that they have no known competing financial interests or personal relationships that could have appeared to influence the work reported in this paper.

Acknowledgements

XH Thanks the support from National Natural Science Foundation of China (NSFC No. 52322610) and PolyU RISDU Joint Research Fund (JRF No. P0058005). YD thanks the support from SFPE Foundation Student Research Grant. This work was also supported in part through the U.S. National Science Foundation's RAPID grant number CCF-2347372. The opinions and perspectives expressed in this study are those of the authors and do not necessarily reflect the views of the sponsor.

Appendix A. Supplementary data

Supplementary data to this article can be found online at https://doi.org/10.1016/j.firesaf.2026.104713.

References

[1] Global Wildfire Information System, Global Wildfire Information System (2024) – with Minor Processing by Our World in Data. https://ourworldindata.org/grapher/annual-number-of-fires, 2025.
[2] W. Tang, C. He, L. Emmons, J. Zhang, Global expansion of wildland-urban interface (WUI) and WUI fires: insights from a multiyear worldwide unified database (WUWUI), Environ. Res. Lett. 19 (2024) 44028.
[3] Y. Kim, Y. Cho, H.K. Heo, L. Lim, Estimating casualties from urban fires: a focus on building and urban environment information, Sustain. Cities Soc. 115 (2024) 105839, https://doi.org/10.1016/j.scs.2024.105839.
[4] Death Count for 2025 LA County Wildfires Likely Higher than Records Show, BU Research Finds. Boston University, August 12, 2025. Retrieved August 20, 2025, https://www.bu.edu/articles/2025/death-count-california-wildfires-higher-than-recorded/.
[5] M. Qiu, D. Chen, M. Kelp, J. Li, G. Huang, The rising threats of wildland-urban interface fires in the era of climate change: The Los Angeles 2025 fires, Innovation 6 (5) (2025) 100835, https://doi.org/10.1016/j.xinn.2025.100835.
[6] F. Szasdi-Bardales, K. Shamsaei, T.W. Juliano, B. Kosovic, H. Ebrahimian, N. Elhami-Khorasani, An offline coupling of fire spread models to simulate the 2021 Marshall Fire, Int. J. Wildland Fire 34 (2025).
[7] X. Sun, M.A. Brown, M. Cox, R. Jackson, Mandating better buildings: a global review of building codes and prospects for improvement in the United States, Wiley Interdiscip. Rev. Energy Environ. 5 (2016) 188–215.
[8] R. Leon, J. Rossberg, Evolution and future of building codes in the USA, Struct. Eng. Int. 22 (2012) 265–269.
[9] S.-Y. Shih, W. Sher, H. Giggins, Assessment of the building code of Australia to inform the development of BIM-enabled code checking system, in: Proc. 19th World Build. Congr. Constr. Soc. 5-9 May, 2013, pp. 1–12.
[10] Y.-Y. Chen, Y.-J. Chuang, C.-H. Huang, C.-Y. Lin, S.-W. Chien, The adoption of fire safety management for upgrading the fire safety level of existing hotel buildings, Build. Environ. 51 (2012) 311–319, https://doi.org/10.1016/j.buildenv.2011.12.001.
[11] A.I. Filkov, V. Tihay-Felicelli, N. Masoudvaziri, D. Rush, A. Valencia, Y. Wang, D. L. Blunck, M.M. Valero, K. Kempna, J. Smolka, J. De Beer, Z. Campbell-Lochrie, F. R. Centeno, M.A. Ibrahim, C.K. Lemmertz, W.C. Tam, A review of thermal exposure and fire spread mechanisms in large outdoor fires and the built environment, Fire Saf. J. 140 (2023) 103871, https://doi.org/10.1016/j.firesaf.2023.103871.
[12] C. Fiorini, H.D. Craveiro, A. Santiago, L. Laím, L.S. da Silva, Parametric evaluation of heat transfer mechanisms in a WUI fire scenario, Int. J. Wildland Fire 32 (2023) 1600–1618.
[13] S.E. Caton, R.S.P. Hakes, D.J. Gorham, A. Zhou, M.J. Gollner, Review of pathways for building fire spread in the wildland Urban interface part I: exposure conditions, Fire Technol. 53 (2017) 429–473, https://doi.org/10.1007/s10694-016-0589-z.
[14] S.L. Manzello, E.I.D. Foote, Characterizing firebrand exposure from wildland–urban interface (WUI) fires: results from the 2007 Angora Fire, Fire Technol. 50 (2014) 105–124.
[15] X. Ju, M. Conkling, M. Hajilou, S. Lin, F. Mostafa, A. Ayyar, A. McDowell, M. Lisano, M.J. Gollner, Laboratory quantification of firebrand generation from WUI fuels for model development, Fire Saf. J. 141 (2023) 103921.
[16] L. Yan, X. Ju, H. Liu, J. Gong, D. Lai, J. Xu, L. Yang, Ignition limits of pine wood building material under the coupling effects of thermal radiation and cross winds, J. Build. Eng. 96 (2024) 110576, https://doi.org/10.1016/j.jobe.2024.110576.
[17] J.L. Urban, J. Song, S. Santamaria, C. Fernandez-Pello, Ignition of a spot smolder in a moist fuel bed by a firebrand, Fire Saf. J. 108 (2019) 102833, https://doi.org/10.1016/j.firesaf.2019.102833.
[18] H.D. Craveiro, C. Fiorini, L. Laím, B. Guillaume, A. Santiago, Experimental and numerical evaluation of a wildland–urban interface fire scenario, Appl. Sci. 13 (2023) 13236.
[19] M. Hajilou, S. Hu, T. Roche, P. Garg, M.J. Gollner, A methodology for experimental quantification of firebrand generation from WUI fuels, Fire Technol. 57 (2021) 2367–2385.
[20] S. Lin, W. Cui, S. Wang, Y. Qin, Y. Chen, Y. Zhang, X. Huang, S.L. Quarles, M. J. Gollner, Susceptibility to ignition of landscaping mulches exposed to firebrand piles or radiation, Fire Saf. J. 154 (2025) 104388, https://doi.org/10.1016/j.firesaf.2025.104388.
[21] Q. Tong, T. Gernay, Mapping Wildfire Ignition Probability and Predictor Sensitivity with Ensemble-based Machine Learning, Springer Netherlands, 2023, https://doi.org/10.1007/s11069-023-06172-x.
[22] A. Maranghides, E.L. Johnsson. Residential Structure Separation Fire Experiments, 2008. https://doi.org/10.6028/NIST.TN.1600.
[23] C.J. Wieczorek, B. Ditch, R.G. Bill, Environmental Impact of Automatic Fire Sprinklers, 2010. http://www.iccsafe.org/gr/Documents/AdoptionToolkit/FM-Global-EnvironmenmtalImpactAutomaticFireSprinklers.pdf.
[24] D.M.J. Purnomo, Y. Qin, M. Theodori, M. Zamanialaei, C. Lautenberger, A. Trouvé, M. Gollner, Reconstructing modes of destruction in wildland–urban interface fires using a semi-physical level-set model, Proc. Combust. Inst. 40 (2024) 105755, https://doi.org/10.1016/j.proci.2024.105755.
[25] Y. Qin, D.M.J. Purnomo, M. Theodori, M. Zamanialaei, C. Lautenberger, M. Gollner, A. Trouvé, Simulations of firebrand-driven fire spread in landscape-scale Wildland-Urban-Interface (WUI) and urban conflagration models, Fire Saf. J. 162 (2026) 104686, https://doi.org/10.1016/j.firesaf.2026.104686.
[26] N. Masoudvaziri, F. Szasdi Bardales, O.K. Keskin, A. Sarreshtehdari, K. Sun, N. Elhami-Khorasani, Streamlined wildland-urban interface fire tracing (SWUIFT): modeling wildfire spread in communities, Environ. Model. Software 143 (2021) 105097, https://doi.org/10.1016/j.envsoft.2021.105097.
[27] S.W. Lee, R.A. Davidson, Physics-based simulation model of post-earthquake fire spread, J. Earthq. Eng. 14 (2010) 670–687, https://doi.org/10.1080/13632460903336928.
[28] D.M.J. Purnomo, Y. Qin, M. Theodori, M. Zamanialaei, C. Lautenberger, A. Trouvé, M. Gollner, Reconstructing modes of destruction in wildland–urban interface fires using a semi-physical level-set model, Proc. Combust. Inst. 40 (2024), https://doi.org/10.1016/j.proci.2024.105755.
[29] Z. Ma, P. Mäkeläinen, Parametric temperature–time curves of medium compartment fires for structural design, Fire Saf. J. 34 (2000) 361–375.
[30] C.R. Barnett, Replacing international temperature–time curves with BFD curve, Fire Saf. J. 42 (2007) 321–327, https://doi.org/10.1016/j.firesaf.2006.11.001.
[31] B.S. Institution, BS EN 1991-1-2. Eurocode 1. Actions on structures: part 1-2. General actions. Actions on Structures Exposed to Fire, British Standards Institution, 2021.
[32] Y. Ding, T. Gernay, X. Li, N. Elhami-Khorasani, S. Xu, X. Huang, AI-Enabled assessment of structural fuel load from street house images in wildland urban interface, Appl. Energy Combust. Sci. (2026) (Under Review).
[33] OpenStreetMap contributors, Planet dump, retrieved from, https://planet.osm.org, 2017.
[34] Microsoft, Nokia, Grand Rapids, MI (Map), Bing Maps, 2025.
[35] F. Szasdi-Bardales, K. Shamsaei, N.P. Lareau, T.W. Juliano, B. Kosovic, H. Ebrahimian, N. Elhami-Khorasani, Integrating dynamic wildland fire position input with a community fire spread simulation: a case study of the 2018 camp fire, Fire Saf. J. 143 (2024) 104076, https://doi.org/10.1016/j.firesaf.2023.104076.
[36] F. Szasdi-Bardales, K. Shamsaei, T.W. Juliano, B. Kosovic, H. Ebrahimian, N. Elhami-Khorasani, An offline coupling of fire spread models to simulate the 2021 Marshall fire, Int. J. Wildland Fire 34 (2025) 1–21, https://doi.org/10.1071/WF24027.
[37] T.W. Juliano, F. Szasdi-Bardales, N.P. Lareau, K. Shamsaei, B. Kosovic, N. Elhami-Khorasani, E.P. James, H. Ebrahimian, Brief communication: the Lahaina fire disaster: how models can be used to understand and predict wildfires, Nat. Hazard. Earth Syst. Sci. Discuss 2023 (2023) 1–7.
[38] S. Santamaria, K. Kempná, J.C. Thomas, M. El Houssami, E. Mueller, D. Kasimov, A. Filkov, M.R. Gallagher, N. Skowronski, R. Hadden, Investigation of structural wood ignition by firebrand accumulation, in: First Int. Conf. Struct. Saf. Under Fire Blast. Glas. UK, 2015, pp. 1–13.
[39] T.E. Waterman. Experimental Study of Firebrand Generation, 1969. https://apps.dtic.mil/sti/tr/pdf/AD0695640.pdf.
[40] J.G. Quintiere. Fundamentals of Fire Phenomena, 2006. https://doi.org/10.1002/0470091150.
[41] Pacific disaster center (PDC) and the federal emergency management agency (FEMA) releases fire damage assessment maps. https://www.mauinuistrong.info/news/pacific-disaster-center-pdc-and-the-federal-emergency-management-agency-fema-releases-fire-damage-assessment-maps, 2023.
[42] W.C. Skamarock, J.B. Klemp, J. Dudhia, D.O. Gill, Z. Liu, J. Berner, W. Wang, J. G. Powers, M.G. Duda, D.M. Barker, A description of the advanced research WRF version 4, NCAR Tech. Note Ncar/Tn-556+ Str 145, 2019.

[43] County of Maui Department of Fire and Public Safety, Origin and cause report. MFD RMS # 23-0012446 and RMS # 23-0012492, Maui County, Accessed April 2025, https://www.mauirecovers.org/news/mfd-and-atf-conclude-aug-8-2023-lahaina-fire-was-one-fire-caused-by-re-energization-of-broken-electrical-line, 2023.
[44] F.J. Szasi-Bardales, Wildfire Damage Assessment in Wildland-Urban Interface Communities, State University of New York at Buffalo, University at Buffalo, NY, U. S, 2025. PhD Dissertation.
[45] Insurance Institute for Business & Home Safety, IBHS Insights: Lahaina Fire – 2023, 2023. https://firesafemarin.org/wp-content/uploads/IBHSEarlyInsights-LahainaFire-1.pdf.
[46] K. Himoto, M. Shinohara, A. Sekizawa, K. Takanashi, H. Saiki, A field experiment on fire spread within a group of model houses, Fire Saf. J. 96 (2018) 105–114, https://doi.org/10.1016/j.firesaf.2018.01.003.
[47] S. Kerber, D. Alkonis, Lahaina fire comprehensive report timeline. https://fsri.org/resource/phase-one-lahaina-fire-comprehensive-timeline-report, 2024.
[48] D.M.J. Purnomo, Y. Qin, M. Theodori, M. Zamanialaei, C. Lautenberger, A. Trouvé, M.J. Gollner, Integrating an urban fire model into an operational wildland fire model to simulate one dimensional wildland-urban interface fires: a parametric study, Int. J. Wildland Fire 33 (2024) 1–17, https://doi.org/10.1071/WF24102.